Ambient Sunlight-Driven High Performance of Chlorinated Volatile Organic Compounds Oxidation by $Cu_{0.15}Mn_{0.15}Ce_{0.7}O_x$ Hollow Spheres

Qixuan Wu,[a]‡ Dachao Yuan,[b]‡ Haixiao Wang,[a]‡ Chenxi Song,[a] Qingqing Guan,[a] Wenjing Wang,[c,]* Yaguang Li,[a,]* Jie Zhao[a,]*

[a.] Research Center of Light Driven Double Carbon, Machine Vision Technology Innovation Center of Hebei Province, The College of Physics Science and Technology, The College of Electronic and Information Engineering, Hebei University, Baoding, 071002, China. E-mail: liyaguang@hbu.edu.cn, Zhaojie_hbu@126.com.

[b.] College of Mechanical and Electrical Engineering, Technology Innovation Center of Intelligent Agricultural Equipment, Hebei Agricultural University, Baoding 071001, China.

[c.] School of Life Sciences, Hebei University, Baoding 071002, China. E-mail: wangwenjing@hbu.edu.cn.

‡These authors contributed equally.

Experimental Sections

Chemical.

Sodium oleate, glucose, ethanol, copper nitrate ($Cu(NO_3)_2$), four hydrated manganese nitrate($Mn(NO_3)_2{\cdot}4H_2O$), six hydrated cerium nitrate ($Ce(NO_3)_3{\cdot}6H_2O$), polyvinyl alcohol (PVA) were purchased from Macklin Co. Ltd. Cerium oxide (CeO_2), copper oxide(CuO), and manganese oxide (MnO_2) was purchased from Aladdin Co. Ltd. All chemicals were of an analytical grade, and used without any more processing.

Preparation of $CuMnCeO_x$

The hydrothermal method was used to create carbon spheres. 0.2 g sodium oleate and 12 g glucose were added to 60 ml deionized water, followed by 2 hours of magnetic stirring. The mixture was transferred to an autoclave, kept at 170 °C for 7 hours. The product was rinsed several times with ethanol and deionized water, collected by centrifugation. Finally, the prepared product was dried at 80 °C and ground to obtain carbon sphere powder.

$CuMnCeO_x$ was synthesized by calcinating premix metal salts with carbon sphere template. Initially, 2 g carbon spheres, 76 mg $Cu(NO_3)_2$, 102 mg $Mn(NO_3)_2{\cdot}4H_2O$ and 822 mg $Ce(NO_3)_3{\cdot}6H_2O$ were added to 10 ml deionized water successively. The mixture was then mixed with 0.5 g PVA and stirred for 2 hours. The obtained solution was freeze-dried overnight using liquid nitrogen. The powder was heat treated in air for 8 hours at 500 °C. A sequence of $CuMnCeO_x$ was prepared by adjust the molar proportion of Cu element, as labeled by the subscript a (0, 0.1, 0.15, 0.2, 0.3). $Cu_aMn_{0.3-a}Ce_{0.7}O_x$ was assigned to the as-prepared catalysts, which included $Mn_{0.3}Ce_{0.7}O_x$,

$Cu_{0.1}Mn_{0.2}Ce_{0.7}O_x$, $Cu_{0.15}Mn_{0.15}Ce_{0.7}O_x$, $Cu_{0.2}Mn_{0.1}Ce_{0.7}O_x$, and $Cu_{0.3}Ce_{0.7}O_x$. Note that the total concentration of metal salt was kept at 100 mg/ml. For comparison, the conventional $Cu_{0.15}Mn_{0.15}Ce_{0.7}O_x$ bulk was prepared and identified as $Cu_{0.15}Mn_{0.15}Ce_{0.7}O_x$-M. The synthesis process of $Cu_{0.15}Mn_{0.15}Ce_{0.7}O_x$-M was the same as $Cu_{0.15}Mn_{0.15}Ce_{0.7}O_x$ but without the carbon sphere and PVA.

Characterizations

Images from a scanning electron microscope (SEM) were captured using an FEI Nova NanoSEM450 instrument. The form and crystal structure of the nanostructures were identified using scanning transmission electron microscopy (STEM, JEOL F200) and energy dispersions spectrometer (EDS) mapping. TEM and HRTEM images were obtained from high resolution transmission electron microscope (JEOL-2100Plus) under 200 kV acceleration voltage. Powder X-ray diffraction (XRD) of the produced materials was performed on A Bede D1 system using Cu Kα radiation (λ = 1.5406 A) at 20 kV and 30 Ma. The specific surface areas were calculated using the Brunauer-Emmett-Teller (BET) method for N_2 adsorption-desorption at 77 K (Beishide 3H-2000PS). The pore size distribution was calculated using the BJH (Barett-Joyner-Halenda) method from the adsorption branch of the isotherms. The EDAX Orbis Micro-XRF instrument was used for elemental analysis of the samples by X-ray fluorescence analysis (XRF). Thermo EscalAB-250 spectrometer with a monochromatic Al Kα radiation source(1486.6 eV) was used to perform X-ray photoelectron spectroscopy (XPS) . The binding energy reported by XPS was adjusted by referring to an indeterminate carbon peak (284.6 eV) for each sample. UV-visible-infrared (IR)

absorption spectra were recorded by Hitachi Limited U4100 and FTIR spectrometer (Bruker, VERTEX 70 FT-IR). Fluke Ti300 infrared thermal imager (USA) was used to take infrared images. A Quantachrome chembet TPR/TPD was used to perform H_2 temperature-programmed reduction (H_2-TPR), O_2 temperature-programmed desorption (O_2-TPD), and NH_3 temperature-programmed desorption (NH_3-TPD). All samples were initially processed at 150 °C for 1 hour in a He atmosphere at 50 mL/min. Following preprocessing, 100 mg samples were heated from 50 to 800 °C at a ramp rate of 10 °C/min while being exposed to 30 mL/min of 10% H_2/He for the H_2-TPR analysis. For O_2-TPD and NH_3-TPD analysis, 100 mg samples after preprocessing were firstly subjected to saturation adsorption at 50 °C for 1 hours while being exposed to 30 mL/min of 5% O_2/He and 7% NH_3/He atmosphere, severally. Following that,100 mg samples were heated from 50 to 800 °C at a ramp rate of 10 °C/min after being purified under 30 mL/min He atmosphere for 1 hour to collect O_2/NH_3 desorption signals from the online mass spectra.

The H_2 uptake, O_2 desorption and NH_3 desorption were calculated by the Eqs. (1) , (2), and (3), respectively.

$$H_2 \text{ uptake } (mmol\ g^{-1}) = \frac{C_{H_2}}{C_1 \times m_1} \times 1000 \quad (1)$$

$$O_2 \text{ desorption } (mmol\ g^{-1}) = \frac{C_{O_2}}{C_2 \times m_2} \times 1000 \quad (2)$$

$$NH_3 \text{ desorption } (mmol\ g^{-1}) = \frac{C_{NH_3}}{C_3 \times m_3} \times 1000 \quad (3)$$

Where, the C_{H_2} and C_1 referred to the standard H_2 concentration tested in advance and the actual H_2 concentration tested with $Cu_{0.15}Mn_{0.15}Ce_{0.7}O_x$ catalyst and

$Cu_{0.15}Mn_{0.15}Ce_{0.7}O_x$-M catalyst, respectively. C_{O_2} and C_2 were the standard O_2 concentration tested in advance and the actual O_2 concentration tested with $Cu_{0.15}Mn_{0.15}Ce_{0.7}O_x$ catalyst and $Cu_{0.15}Mn_{0.15}Ce_{0.7}O_x$-M catalyst, respectively. $C_{NH_3}$and C_3 were the standard NH_3 concentration tested in advance and the actual NH_3 concentration tested with $Cu_{0.15}Mn_{0.15}Ce_{0.7}O_x$ catalyst and $Cu_{0.15}Mn_{0.15}Ce_{0.7}O_x$-M catalyst, respectively. m_1, m_2, and m_3 were the mass of catalyst used for H_2-TPR, O_2-TPD and NH_3-TPD tests, respectively.

The temperature range of the test is 50-800 °C."

Thermal catalytic test

The thermal catalytic exercise of catalysts for CB combustion was examined by the fixed-bed reactor (XM190708-007, Dalian Zhongjiaruilin Liquid Technology CO., Ltd) in the non-stop flow form. Typically, a quartz flow reactor held 200 mg of catalyst. CB was injected into the reactor by bubbling the saturated aqueous solution of CB at 25 °C with dried clean air (21% O_2 + 79% N_2) as the carrier gas. The concentration of CB in the input gas was measured to be 1000 ppm. The total input gas flow was maintained at 50 sccm. The samples were heated from 25 °C to 500 °C at a ramp rate of 5 °C/min. The reaction products were examined using as a gas chromatograph (GC) 7890A geared up with FID and TCD detectors. The CB conversion ($CB_{conv.}$), CB conversion rate (r_{CB}) and CB selectivity ($CB_{sel.}$) were calculated by the Eqs. (4), (5), and (6), respectively. As the catalyst mass and reaction time varied in different research works, the CB conversion rate (mmol g^{-1} h^{-1}) was calculated for comparison.

$$CB_{conv.}\,(\%) = \left(\frac{C_{CB,\ in} - C_{CB,out}}{C_{CB,in}}\right) \times 100\% \quad (4)$$

$$r_{CB}\,(mmol\ g^{-1}h^{-1}) = \frac{C_{CO_2} \times L \times 60}{G} \times \frac{1}{6} \quad (5)$$

$$CB_{sel.}\,(\%) = \left(\frac{C_{CO_2}}{C_{CO_2} + C_{CO}}\right) \times 100\% \quad (6)$$

Where the $C_{CB,\ in}$ and $C_{CB,out}$ referred to the concentrations of CB before and after reaction, respectively. C_{CO_2} and C_{CO} were the concentrations of CO_2 and CO measured by GC, respectively. L was the flow rate of outlet dry gas (50 sccm), and G was the mass of catalyst.

Photothermal catalytic test

The light source of photothermal tests was provided by simulated sunlight equipment (HP-2-4000, Hebei Saichi Co. Ltd). The uniform irradiation area of light source was 0.8 m * 0.3 m with adjustable light intensity. 100 mg catalyst was placed into the designed reactor of photothermal tube. The gas mixture containing 1000 ppm CB and dried clean air (21% O_2 + 79% N_2) was fed into the photothermal tube. The flow rate of feed gas was 100 sccm, and reactor was exposed under light irradiation to start the reaction. The reaction products were examined using as a gas chromatograph (GC) 7890A geared up with FID and TCD detectors. The photocatalytic oxidation of $Cu_{0.15}Mn_{0.15}Ce_{0.7}O_x$ was performed in a quartz tube instead of the photothermal tube, while maintaining the other test conditions.

Table S1. Crystal size of $Cu_{0.15}Mn_{0.15}Ce_{0.7}O_x$-M and $CuMnCeO_x$ with different metal ratios using Scherrer equation for peak (111).

Samples	Bragg angle θ (°)	B (radian×10^{-3})	Crystal size for peak (111) (nm)
$Cu_{0.1}Mn_{0.2}Ce_{0.7}O_x$	28.8240	1.67731	5.11147
$Cu_{0.15}Mn_{0.15}Ce_{0.7}O_x$	29.02181	2.36635	3.62471
$Cu_{0.2}Mn_{0.1}Ce_{0.7}O_x$	28.79405	0.63896	13.41703
$Cu_{0.3}Ce_{0.7}O_x$	28.820601	0.7292	11.75749
$Mn_{0.3}Ce_{0.7}O_x$	28.8614	1.7683	4.84886
$Cu_{0.15}Mn_{0.15}Ce_{0.7}O_x$-M	28.77671	0.21437	39.98981

Table S2. Elemental compositions of synthesized catalysts.

Elements	$Cu_{0.15}Mn_{0.15}Ce_{0.7}O_x$	$Cu_{0.15}Mn_{0.15}Ce_{0.7}O_x$-M
Ce	70.75%	68.7%
Mn	17.03%	18.02%
Cu	12.22%	13.28%

Table S3. Textual properties of synthesized catalysts.

Samples	BET surface area (m^2 g^{-1})	Cumulative pore volume (cm^3 g^{-1})
$Cu_{0.15}Mn_{0.15}Ce_{0.7}O_x$	157.19	0.3809
$Cu_{0.15}Mn_{0.15}Ce_{0.7}O_x$-M	86.98	0.1782

Table S4. Distribution of Mn ions, Ce ions, and O species of synthesized catalysts based on XPS results.

Samples	Mn^{4+} (%)	Ce^{3+} (%)	O_{ads}/O_{latt}
$Cu_{0.15}Mn_{0.15}Ce_{0.7}O_x$	55	11	0.48
$Cu_{0.15}Mn_{0.15}Ce_{0.7}O_x$-M	25	7.5	0.28
$Cu_{0.15}Mn_{0.15}Ce_{0.7}O_x$-used	28	12	0.26

Table S5. H_2 uptake, O_2 desorption, and NH_3 desorption of synthesized catalysts.

Samples	H_2 uptake (mmol g^{-1})	O_2 desorption (mmol g^{-1})	NH_3 desorption (mmol g^{-1})
$Cu_{0.15}Mn_{0.15}Ce_{0.7}O_x$	0.4026	0.0306	0.6899
$Cu_{0.15}Mn_{0.15}Ce_{0.7}O_x$-M	0.1435	0.0212	0.5313

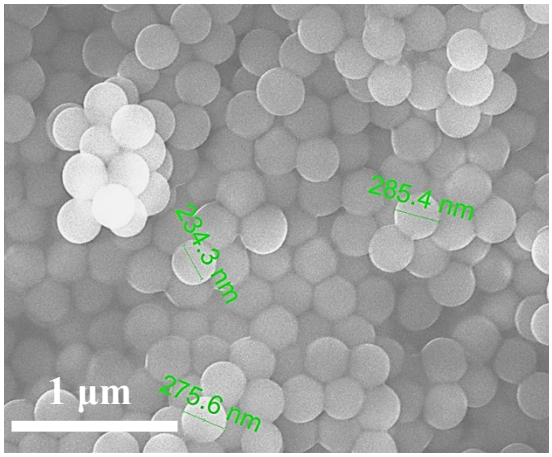

Fig. S1. SEM image of carbon spheres.

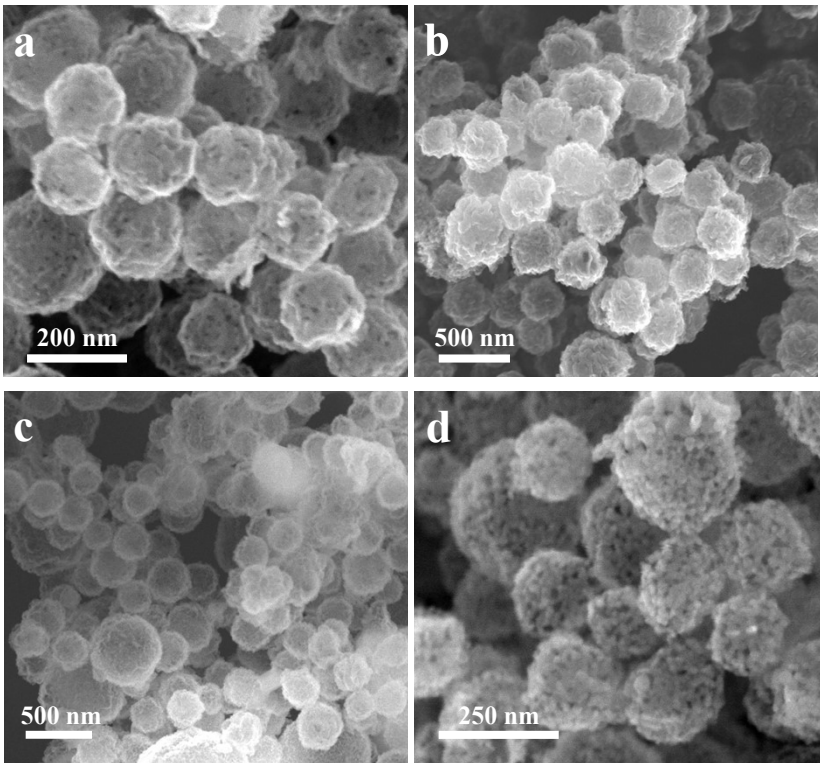

Fig. S2. SEM images of (a) $Cu_{0.1}Mn_{0.2}Ce_{0.7}O_x$, (b) $Cu_{0.2}Mn_{0.1}Ce_{0.7}O_x$, (c) $Cu_{0.3}Ce_{0.7}O_x$, (d) $Mn_{0.3}Ce_{0.7}O_x$.

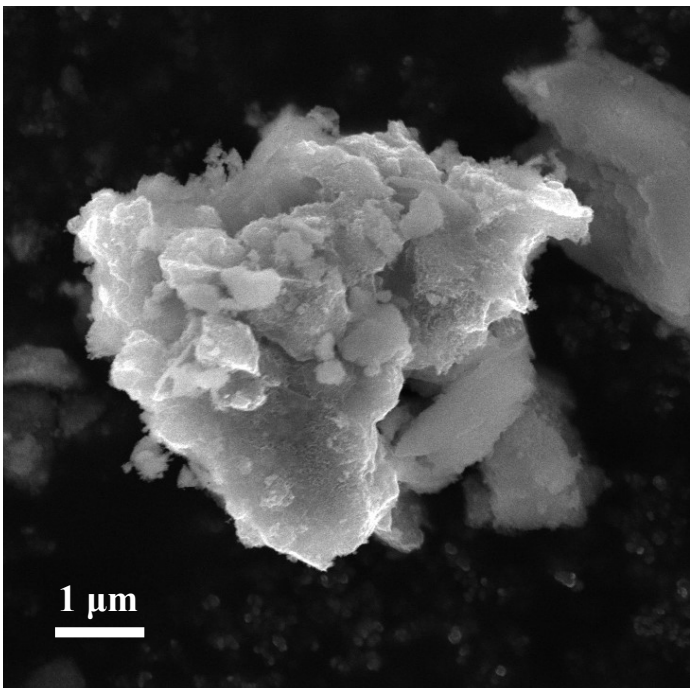

Fig. S3. SEM image of $Cu_{0.15}Mn_{0.15}Ce_{0.7}O_x$-M.

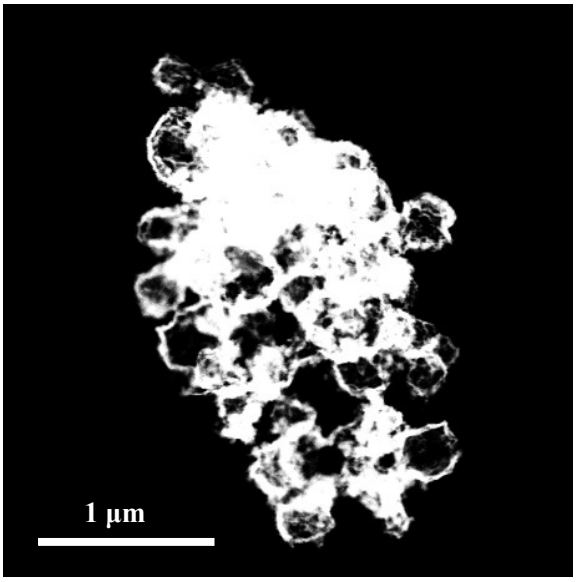

Fig. S4. TEM-EDS image of $Cu_{0.15}Mn_{0.15}Ce_{0.7}O_x$.

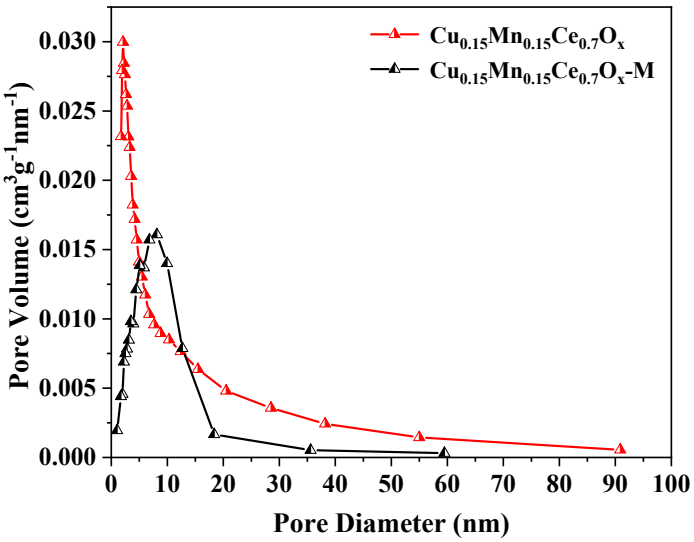

Fig. S5. Pore distributions of $Cu_{0.15}Mn_{0.15}Ce_{0.7}O_x$ and $Cu_{0.15}Mn_{0.15}Ce_{0.7}O_x$-M.

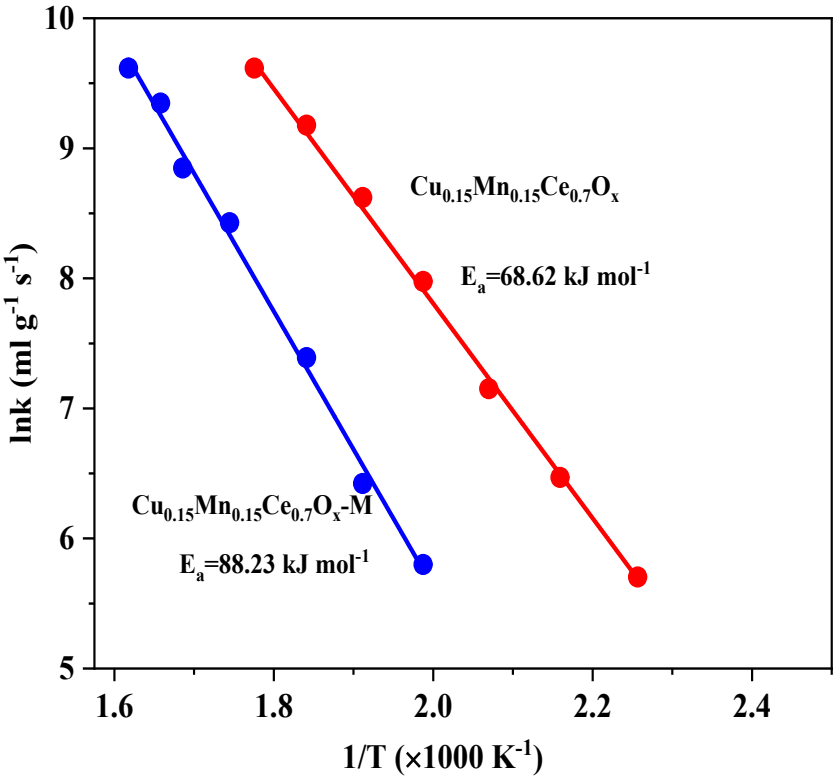

Fig. S6. Activation energies for CB oxidation by $Cu_{0.15}Mn_{0.15}Ce_{0.7}O_x$ and $Cu_{0.15}Mn_{0.15}Ce_{0.7}O_x$-M.

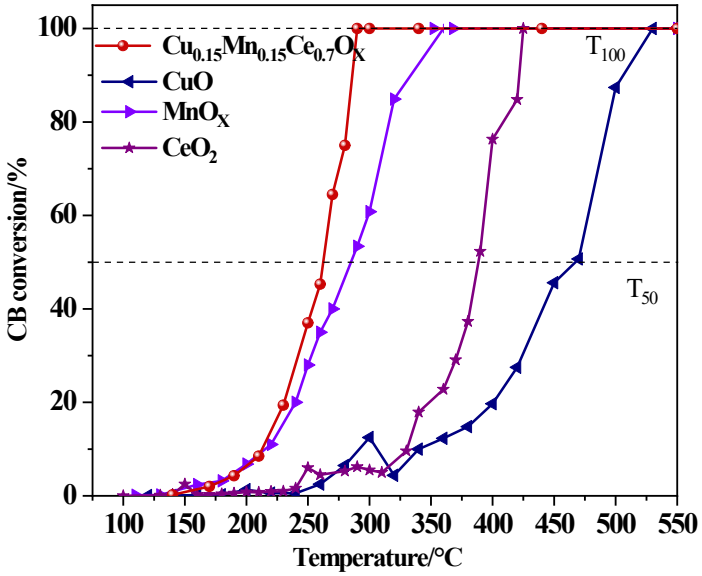

Fig. S7. CB conversion rates of $Cu_{0.15}Mn_{0.15}Ce_{0.7}O_x$, CuO, MnO_2, and CeO_2.

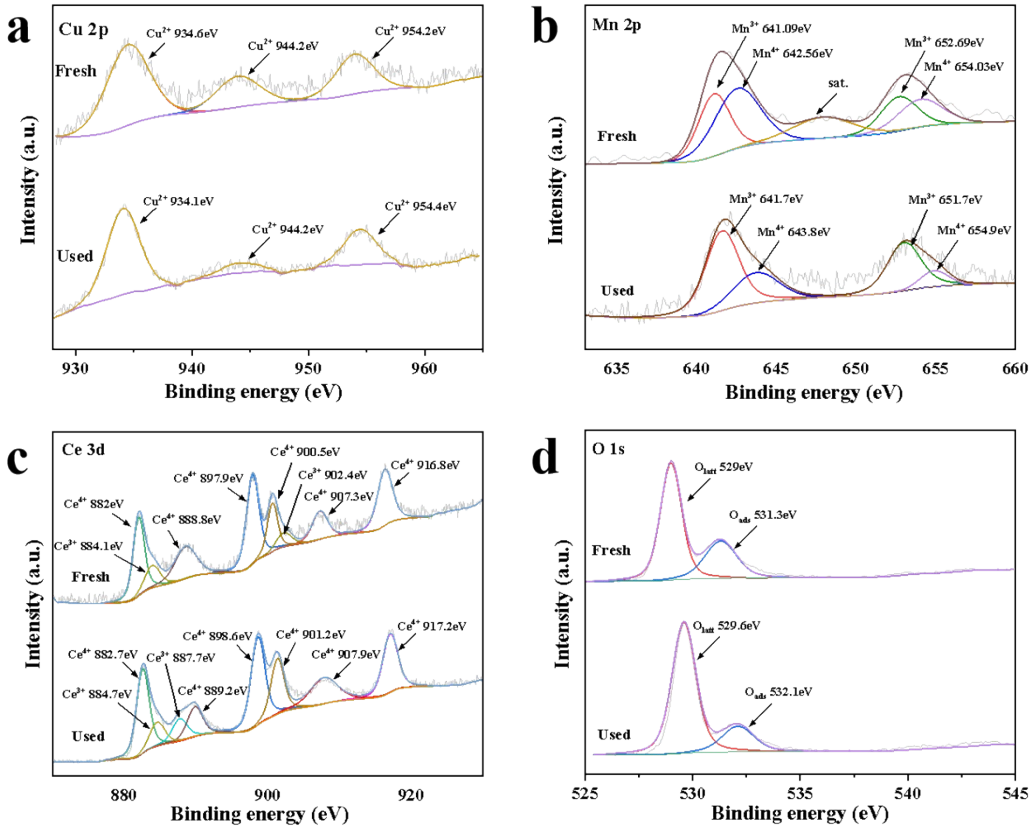

Fig. S8. (a) Cu 2p, (b) Mn 2p, (c) Ce 3d, and (d) O 1s XPS of $Cu_{0.15}Mn_{0.15}Ce_{0.7}O_x$ before and after reaction.

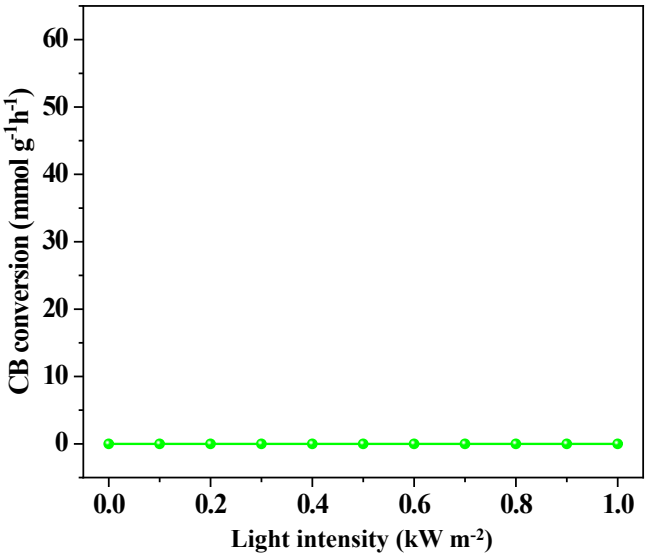

Fig. S9. CB conversion rate of $Cu_{0.15}Mn_{0.15}Ce_{0.7}O_x$ under different intensities of solar irradiation (test conditions: 100 mg catalysts, 1000 ppm CB, 100 sccm feed gas of 21% O_2 and 79% N_2)

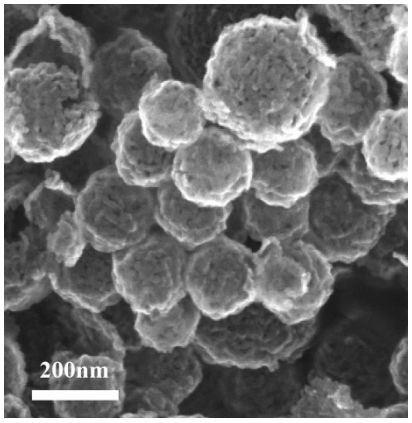

Fig. S10. SEM image of the $Cu_{0.15}Mn_{0.15}Ce_{0.7}O_x$ catalyst after 48 hours of stability.